AIAA 81-0040R

Combustion Characteristics of High-Pressure Gas-Fired Combustors

Essam Eldin Khalil*
Cairo University, Cairo, Egypt

The present work describes a mathematical procedure for predicting the local properties in combustors characterized with high combustion intensity and high pressure. Turbulence is represented by the *k-e* model. The combustion model assumes a single-step reaction and solves the conservation equations for the mass fraction of the fuel and the square of its fluctuation and the density-velocity and density-scalar fluctuation correlations. A new density correction term is included in the pressure correction procedure to account for high combustor pressures. Calculated results are compared to experimental data obtained in a gas-fired combustor; the merits and drawbacks of the present models are discussed.

Nomenclature

A	= area
D_f	= furnace diameter
e	= dissipation rate of turbulent kinetic energy
f	= mixture fraction
k	= kinetic energy of turbulence
M_{fu}, M_{ox}	= fuel and oxygen mass fractions
P	= pressure
$P(M_{fu})$	= probability distribution of fuel mass fraction
r	= radius
$S(\theta)$	= source term of the entity θ
T	= gas temperature
U_j	= velocity components in the x_j coordinate direction, $j=1,2,3$
u_j	= velocity fluctuation components
U, V, W	= axial, radial, and tangential velocity components
x	= axial distance from the burner exit
ρ	= density
Γ_θ	= turbulent exchange coefficient
μ	= viscosity
θ	= general dependent variable
φ	= fluctuating component of θ

Subscripts

eff	= effective (including the effects of turbulence)
fu	= fuel
ox	= oxygen

Superscripts

$(\ )'$	= fluctuations
$(\bar{\ })$	= mean value

Introduction

NUMERICAL investigations have covered a wide field of engineering applications. Aerodynamic characteristics, reaction characteristics, and heat transfer all have been calculated by solving the conservation equations that govern the transport of mass, momentum, and energy. The procedure that is followed is well documented (see Refs. 1-4). The fact that these calculations can provide the necessary information for the design of a great number of engineering purposes (e.g., gas turbine combustors and fire tube boilers), at a cost lower than that of setting an experimental program, cannot be sufficiently emphasized.

In this present work, the same path of numerical calculations is followed except that, in this case, attention is focused on turbulent flames characterized by high pressure. To represent the turbulence characteristics, the two-equation turbulence model was used. This model employs the kinetic energy of turbulence and its dissipation rate; the shear stresses are represented in terms of an effective viscosity and mean velocity gradients.[5] Naturally, obtaining the Reynolds and shear stresses can be done by solving their transport equations[6]; however, this approach requires large storage space on the computer.

To represent the reaction characteristics, certain assumptions must be made in order to solve the conservation equations of energy and fuel mass fraction. Normally, in diffusion flames the reaction is assumed to be infinitely fast; the effect of the fluctuations was handled differently by several investigators.[7-10] These were examined critically by Khalil.[11] For premixed flames the reaction rate is assumed finite, and again the fluctuations were taken into account.[6,9] To represent the radiative heat transfer, the discrete ordinate model of Khalil et al.[12] was used.

The second section describes the calculation procedure and the modeling assumptions. In the third section, the results of the computations and comparisons with experimental data are presented and discussed to bring into focus the merits of the present procedure as a design tool.

Calculation Procedure

Governing Equations

The conservation equations of mass, momentum, species, and energy that govern the type of flow considered in the present investigation are elliptic in nature. The present computational scheme solves the time-averaged form of these equations. Expressed in finite difference form, this time-averaged form is:

$$\frac{\partial}{\partial x_j}\bar{\rho}\bar{U}_j\bar{\theta} = -\frac{\partial}{\partial x_j}\bar{\rho}\overline{u_j\varphi} + \overline{S(\theta)} \qquad (1)$$

The general dependent variable θ can represent the three velocity components, kinetic energy of turbulence, dissipation rate, stagnation enthalpy $\bar{H}$, fuel mass fraction $\bar{M}_{fu}$, and the square of its fluctuation $\overline{m_{fu}^2}$.

In the above equation, the laminar diffusion term was neglected due to its very small contribution relative to the

Presented as Paper 81-0040 at the AIAA 19th Aerospace Sciences Meeting, St. Louis, Mo., Jan. 12-15, 1981; submitted March 4, 1981; revision received Sept. 14, 1981.

*Lecturer, Dept. of Mechanical Engineering, Faculty of Engineering.

contribution of the turbulent diffusion terms $\overline{u_j\varphi}$. These terms resulted from the time averaging of the instantaneous equations, and they represent the correlations between the velocity components and any scalar entity. In the momentum equations, these terms are the shear and Reynolds stresses, which are commonly evaluated with the aid of the turbulence model closures. For other quantities, the turbulent diffusion terms are expressed in terms of an exchange coefficient and the gradient of the entity $\bar{\theta}$. The values of the term $\overline{S(\theta)}$ denote the source of generation/destruction of the various entities, $\bar{\theta}$. The values of the turbulent exchange coefficient and the source terms are of the form given in Refs. 2, 4, 5, and 11.

As mentioned earlier, since the governing conservation equations are elliptic in nature, the specification of the boundary conditions along the four boundaries of the solution domain is essential to yield the equations soluble. The solution domain conforms, in axisymmetric flows, to a symmetrical half-section of the combustor. The prevailing boundary conditions correspond to the measurements wherever possible. On the combustor walls, velocities are assumed zero and temperatures obtained from measured values. Wall functions,[5] which are based on the logarithmic law of the wall, are used to link the wall values to the near-wall nodal points. Inlet and exit conditions are either specified from the corresponding measurements or reasonably assumed in accordance with the recommendations of Ref. 14.

Physical Modeling

To render the solution of Eq. (1) possible, some of the terms need modeling. These terms are the ones pertaining to turbulence, combustion, and radiation transfer characteristics. Appropriate models are employed for each of these characteristics; in this section, these models are discussed in terms of their accompanying assumptions, formulation, and assessment.

Turbulence Model

During the modeling of the time-averaged Navier-Stokes equations, information about the turbulence nature of the flow is lost; the turbulence model assumptions serve as an approximation. The turbulence model should, however, provide the unknown correlation terms $\overline{u_iu_j}$ in terms of the mean flow entities. Two main approaches were proposed. First, the transport equations for the Reynolds stresses $\overline{u_iu_j}$ can be solved in order to yield the local values of the stress at all grid nodes in the solution domain. This category of models is commonly known as the Reynolds stresses closure and was suggested by Launder et al.[15] and Pope,[6] among others.

The second approach is simpler and fosters the eddy viscosity concept; that is, the Reynolds stresses and shear stresses are expressed in terms of an effective viscosity and mean velocity gradients.

$$\bar{\rho}\overline{u_iu_j} = \frac{2}{3}\left(\bar{\rho}k - \frac{\mu_{\text{eff}}}{\bar{\rho}}\bar{U}_\ell\frac{\partial\bar{\rho}}{\partial x_\ell}\right)\delta_{ij} - \mu_{\text{eff}}(\partial\bar{U}_i/\partial x_j + \partial\bar{U}_j/\partial x_i) \quad (2)$$

and

$$\delta_{ij}=0 \quad \text{for } i\neq j \qquad \text{and} \qquad \delta_{ij}=1 \quad \text{for } i=j$$

where i, j, and ℓ are indices.

This turbulence model is based on the solution of transport equations for k and e. The values of k and e are used to calculate the effective viscosity according to

$$\mu_{\text{eff}} = \mu + 0.09\bar{\rho}k^2/e \quad (3)$$

The former model was tested for boundary layer and shear flows,[15] but no adequate assessment of its behavior in turbulent recirculating reacting flows was reported to date. In contrast, the validity of the latter was extensively tested for reacting and nonreacting flows in Refs. 2, 3, and 5. The constants of the model are those of Hutchinson et al.[2] and were kept unchanged. The values of the turbulent exchange coefficients for k and e are 1.0 and 1.22 times the effective viscosity, respectively.

The present turbulence model is supplemented with two transport equations for the entities $\overline{\rho' u}$ and $\overline{\rho' v}$. These entities appear in the conservation equations as additional mass fluxes, due to fluctuations which convect the entity $\bar{\theta}$. These terms can be treated in three different ways. The first and easy way is to neglect these entities. Second, they can be calculated from the solution of the transport equations.[2,9,10] The third alternative is that these terms can be obtained from algebraic forms of the transport differential equations.[2] In the vicinity of reaction zones, density gradients are very steep and the density-velocity correlations have significant influences and should not be neglected.[10,11]

Reaction Model

The present combustion model assumes that fuel and oxidant react in a single-step irreversible reaction and the rate of reaction at which the fuel disappears is expressed as:

$$S(M_{\text{fu}}) = -10^{10}\rho^2 M_{\text{fu}} M_{\text{ox}} \exp(-1.84\times10^4/T) \quad (4)$$

The time-averaged reaction rate is obtained from the integration of the product of the rate of reaction and the local value of the probability density function of fuel mass fraction, $\overline{P(M_{\text{fu}})}$ as

$$\overline{S(M_{\text{fu}})} = \int_0^{M_0} S(M_{\text{fu}})\overline{P(M_{\text{fu}})}\,dM_{\text{fu}} \quad (5)$$

The present model calculates the local values of the probability $\overline{P(M_{\text{fu}})}$ from the solution of the transport equation of the probability.[6] This transport equation is expressed as

$$\bar{\rho}\frac{D}{Dt}\overline{P(M_{\text{fu}})} = \underbrace{\frac{\partial}{\partial x_j}C_3\bar{\rho}\frac{k^2}{e}\frac{\partial}{\partial x_j}\overline{P(M_{\text{fu}})}}_{\text{(I)}\qquad\text{(II)}} - \underbrace{\frac{\partial}{\partial M_{\text{fu}}}\left[\overline{P(M_{\text{fu}})}S(M_{\text{fu}}) + C_4\bar{\rho}\frac{e}{k}\overline{M_{\text{fu}}^2}\frac{\partial}{\partial M_{\text{fu}}}\overline{P(M_{\text{fu}})}\right]}_{\text{(III)}\qquad\text{(IV)}} \quad (6)$$

The constants C_3 and C_4 equal 0.127 and 0.92, respectively. The local oxygen mass fraction, temperature, and density can be expressed in terms of the fuel mass fraction with the knowledge of the stoichiometric air/fuel ratio and initial air/fuel mass ratio. Local values of $\overline{M_{\text{fu}}^2}$ are obtained from the solution of the corresponding transport equation in the form 1. It should be emphasized here that the source term of $\overline{M_{\text{fu}}^2}$ equation contains terms that represent the effect of chemical reaction on the fluctuation level.[4]

The probability distribution $\overline{P(M_{\text{fu}})}$ is shown to depend strongly on the local reaction rate and the local turbulence properties. The two terms III and IV represent the transport of $\overline{P(M_{\text{fu}})}$ in the M_{fu} space due to chemical reaction and molecular action, respectively.

An alternative approach to determination of $\overline{P(M_{\text{fu}})}$ is to assume the distribution to match one of the common forms of delta functions, beta function, and clipped Gaussian distribution.[2,6] This approach is criticized for its over-simplifying nature, and that no adequate experimental evidence exists to support such distributions in reacting flows.

The turbulent diffusion terms in Eq. (1) are modeled in the algebraic gradient-type form as

$$\bar{\rho} \overline{u_j \varphi} = -\Gamma_\theta \frac{\partial \bar{\theta}}{\partial x_j} \tag{7}$$

The values of the turbulent exchange coefficients Γ_θ are commonly expressed in terms of the effective viscosity μ_{eff}.

The thermodynamic properties of the mixture of gases were obtained using the perfect gas laws, together with fitting the specific heat of the gases to a third-order polynomial. The equation of state was used to obtain the local density from prevailing values of pressure, temperature, and mixture composition.

Heat-Transfer Model

In furnaces and combustion chambers, heat transfer to the walls is an important feature; furnaces with improved rate of heat transfer are always design assets. To calculate the radiative heat flux contribution to the total energy balance, the discrete ordinate radiation model[12] is used which yields the source of energy due to thermal radiation in terms of radiation intensity in discrete directions spanning the solid angle of 2π. The convective heat transfer at the wall is obtained from a gradient-type expression of the form of Eq. (7).

Solution Procedure

The differential equations represented by Eq. (1) were solved in finite difference form by the algorithm of Ref. 16. The solution is based on a guess-and-correct procedure of the local velocity field, and the resulting velocities do not satisfy the continuity equation. Continuity is then enforced and the mass imbalance is used to obtain pressure corrections through the use of a combination of momentum and continuity equations, with a pressure correction equation of the form 1. The new velocity and pressure fields are used as the new guessed fields. The process is repeated until the residuals in all the conservation equations are less than 0.01% of the inlet values.

The new updated velocity is expressed for isothermal and reacting flows at atmospheric pressures as

$$U_j = U_j^* + D_j (P_p' - P_{x_j}') \tag{8}$$

The x_j direction contribution to the net efflux of mass is expressed as:

$$(AU_j\rho)_{x_{j+}} - (AU_j\rho)_{x_{j-}}$$

For pressure-dependent density calculations for compressible flows, such as the one considered here, the density is given as:

$$\rho = \rho^* + (1/a^2)(P_{x_j}' + P_p')/2 \tag{9}$$

where a is the velocity of sound, subscript p refers to any nodal point, x_j refers to the north, south, east, and west nodes, P' refers to the pressure correction, and the starred entities are the guessed values from the previous iteration. The mass flux is calculated as:

$$(\rho A U_j)_{x_j} = (\rho^* U_j^* + (\rho^* D_j + (U_j^*/2a^2))P_p' - (\rho^* D_j - (U_j^*/2a^2))P_{x_j}')A \tag{10}$$

where the terms D_j are the pressure difference coefficients. Equation (10) was used in the present work because of the high pressure combustor flows that are investigated. The updated mass velocity field is then obtained from Eq. (10).

The present computations were performed with a nonuniform grid composed of 20×22 grid nodes. The cost of the calculation is not, however, negligible, since the required computer storage is 38 kilowords and the computation time on the ICL 2956 computer was around 35 min. It is worthwhile to note that the calculations obtained with the neglect of the density-velocity fluctuations require 36 kilowords and the computing time was 32 min. A converged solution was obtained when the maximum normalized residuals in all the conservation equations together with the continuity were less than 0.01% at all grid nodes. The solution of the finite-difference form of Eq. (1) was underrelaxed to aid speedy convergence; underrelaxation parameters of the order of 0.5 for velocities and 0.7 for other scalar entities were used. Grid independence tests were performed and the results described in this work were independent of the grid size and location, in the sense that 50% increase of the grid size would result in less than 7% change in the mean flow pattern results. Further details of grid size effects can be found in Ref. 14.

Results and Comparisons

The comparisons in this section between measured and calculated properties are intended to demonstrate the influence of the density fluctuation terms on the flow pattern and reaction and to assess the validity of the present numerical procedure in solving for high-pressure reacting flows. Two different flame situations in the furnace of Spadaccini et al.[13] have been selected as the basis for these comparisons. The two sets of measurements were obtained in confined diffusion flame configurations and correspond to two different swirl intensities.

The present combustor is an axisymmetric one in which a central fuel stream, natural gas, mixes with a coaxial annular airstream. In the nonswirling flame situation, flame stabilization was achieved by judicious selection of the momentum flux ratio of the fuel and airstreams. This flame-holding approach does not rely either on a physical flame holder (baffle) or on swirling action. For the case with finite swirl number, tangential momentum was imparted to the combustion air through the use of straight swirl vanes.

The combustor diameter was 0.122 m and its length was 1.22 m. An extension section 0.334 m long was also used to fully contain the flame; the coaxial burner described above comprised a central jet of 0.0630 m and an annulus i.d. of 0.0637 m and o.d. of 0.0937 m. The combustor pressure for the present comparisons was 3.8 bar. The airflow rate through the annular space was adjusted to give air to natural gas velocity ratio of 22 and to allow for 10% excess air. The furnace walls were water-cooled in five segments of equal length; the water flow to each zone was independently set to keep the furnace walls at an approximate temperature of 500 K. The furnace was thermally lagged to prevent heat loss to the atmosphere.

The axial and tangential velocity profiles were measured with the aid of a laser Doppler anemometer. For this purpose, the furnace walls were provided with window ports to allow the optical velocity measurements. The measurements comprised the mean and fluctuating components of each velocity. The anemometer was designed to be able to measure the regions of flow reversal; a crystal Bragg cell was used as a beam splitter and for frequency shifting. The mean velocity measurements were subjected to possible experimental errors up to 5%, except in the vicinity of the recirculation zone where errors increase to 30%.

Temperature profiles at the exit plane and within the combustor were measured by traversing a calibrated heat-loss thermocouple probe across the combustor. Local gas temperatures were obtained from the reading of a thermocouple, which was corrected for conduction and radiation heat losses. The experimental accuracy in this case lies within ± 30 K. Further details of the measuring technique and the associated errors can be found in the original papers by Spadaccini et al.[13] and Bowman et al.[17] Species concentration distributions

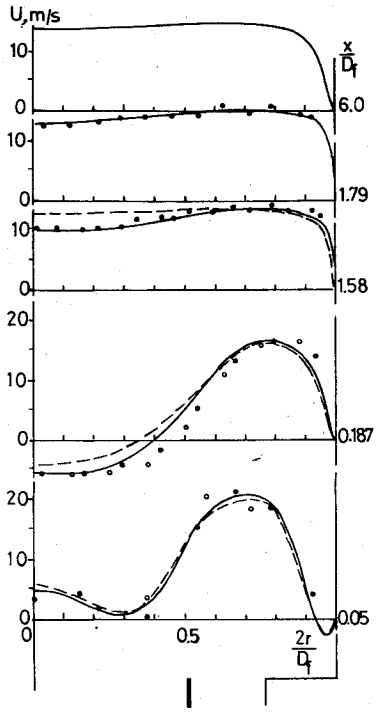

Fig. 1 Measured and calculated axial velocity profiles in a high-pressure combustor, zero swirl. ○, ● measurements in each half-section of the combustor of Ref. 13; —— present calculations; ---- calculations without density fluctuation and pressure terms.

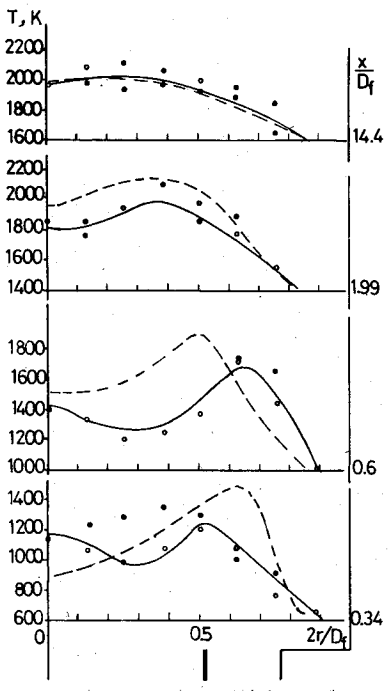

Fig. 2 Measured and calculated gas temperature profiles in a high-pressure combustor, zero swirl. ○, ● measurements in each half-section of the combustor of Ref. 13; —— present calculations; ---- calculations without density fluctuation and pressure terms.

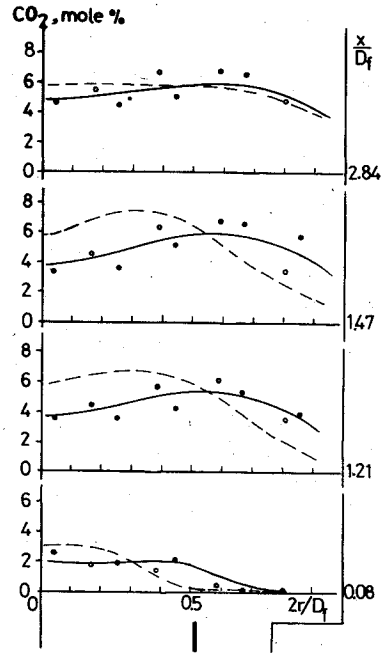

Fig. 3 Measured and calculated carbon dioxide profiles in high-pressure combustor, zero swirl. ○, ● measurements in each half-section of the combustor of Ref. 13; —— present calculations; ---- calculations without density fluctuation and pressure terms.

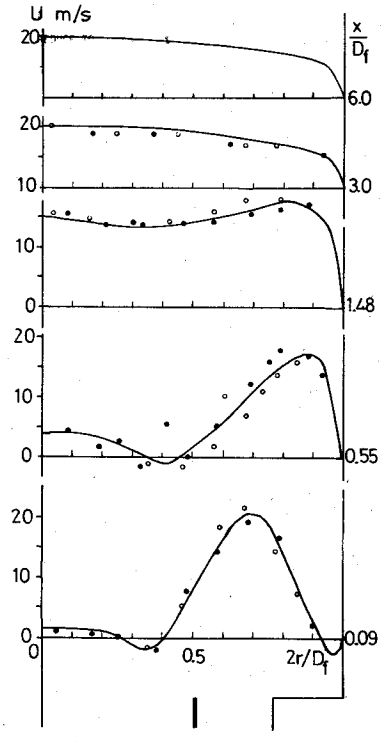

Fig. 4 Measured and calculated axial velocity profiles in a high-pressure combustor, swirl number = 0.3. ○, ● measurements in each half-section of the combustor of Ref. 13; —— present calculations.

within the combustor were measured using a traverse gas sampling probe and an exhaust gas sampling rake. The associated errors in gas sampling technique are estimated to be less than 5%. The radial distribution of the time-averaged velocity at inlet is measured with a pitot probe. No measurements of the inlet profiles of turbulent kinetic energy and its dissipation rate were reported; hence, they were assumed according to the recommendations of Ref. 14. Using a uniform inlet profile of k and e changes the value of the velocities by 10% than that predicted here using a turbulent pipe flow profile for k and e.

The calculated flow properties are compared with the corresponding measurements in the following paragraphs. The calculated and measured profiles of mean axial velocity component for the nonswirling flame situation are shown in Fig. 1. The agreement between the measurements and the

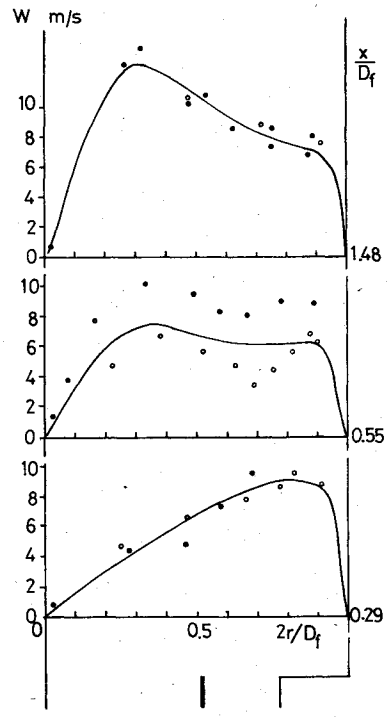

Fig. 5 Measured and calculated tangential velocity profiles in a high-pressure combustor, swirl number = 0.3. ○, ● measurements in each half-section of the combustor of Ref. 13; —— present calculations.

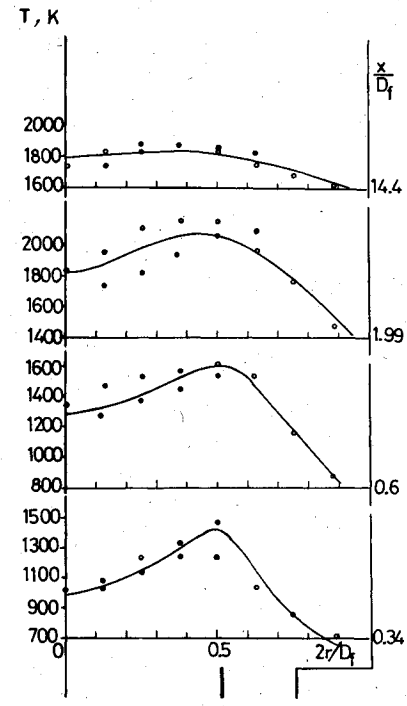

Fig. 6 Measured and calculated gas temperature profiles in a high-pressure combustor, swirl number = 0.3. ○, ● measurements in each half-section of the combustor of Ref. 13; —— present calculations.

calculations is reasonable, as the calculated velocity profiles predicted correctly the rate of spread of the jet and the decay of the centerline mean velocity. The small expansion ratio of 1:1.3 naturally created a very small wall recirculation zone. The central recirculation zone was created by the momentum exchange between the high velocity airstream and the low velocity fuel stream. On the same figure, the calculated velocity profiles are shown when the density-velocity correlations were neglected and no account was taken for the high-pressure effect on the solution algorithm. It is evident then that the difference shown attributed to these effects, and that the present modifications, i.e., the inclusion of the density fluctuation correlations, yield better agreement.

Measured and calculated gas temperature profiles are shown in Fig. 2 for the same flow situation, and exhibited reasonable agreement except in the vicinity of the burner exit. Maximum discrepancies of less than 10% of the local temperature were observed; however, the agreement obtained is satisfactory for engineering purposes. On the same figure, it is clear that the predicted gas temperature profiles, obtained with the neglect of the density fluctuation correlations, are in poor agreement with the measurements, particularly in the vicinity of the reaction zone. Such discrepancy is attributed to the large density gradients and hence large production rate of density fluctuations and density-velocity correlations. It can be seen that the neglect of such terms, particularly in a high-pressure combustor, results in serious defects in predicting the flame dimensions and heat release and transfer. Accurate calculations of nitric oxide concentrations are based on adequate predictions of local gas temperatures; hence, the inclusion of the density-velocity correlations is vital for pollutant calculations.[2]

The measured and calculated profiles of mean carbon dioxide concentrations are shown in Fig. 3 at various axial locations downstream of the burner. On the whole, the obtained agreement was satisfactory. It was observed that the profiles flatten out at further downstream locations, thus identifying the end of the reaction where the CO_2 mole concentrations increased to the complete combustion values. The calculated carbon dioxide concentration profiles, obtained with the neglect of the density-velocity correlation terms, are also shown on the same figure. The large discrepancies between such calculations and the measurements are attributed to predicting lower levels of turbulence and narrower flame than those measured. The predicted convection of carbon dioxide along the flame axis is much larger than measured values in contrast to that predicted when the correlation terms are included.

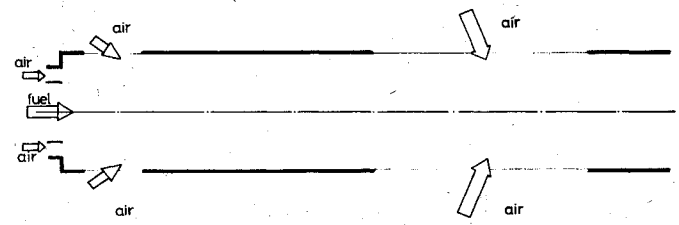

Fig. 7 Axisymmetric combustor with circumferential air dilution.

The second set of comparisons pertains to a swirling flame situation where the swirl number was 0.3. The introduction of swirl resulted in off-center recirculation zones, as can be seen in Fig. 4, where the measured and calculated mean axial velocity profiles are compared. Both measurements and predictions were in reasonable agreement except in the vicinity of recirculation zones. The calculations were repeated, but, in this case, the density fluctuation terms and the effect of combustor pressure (3.8 bar) were neglected; the calculated flowfield did not show any recirculation zones, which is contrary to the experimental observations.

Calculated profiles of mean tangential velocity and the corresponding measurements are shown in Fig. 5 at various axial locations. The tangential velocity profiles exhibited an off-center peak; the maximum tangential velocity was less than 15% of the maximum inlet velocity. The observed discrepancies of Fig. 5 were less than 10% and can be attributed partially to the turbulence model. It should be noted that the W profile changed from forced to Rankine vortex flow.

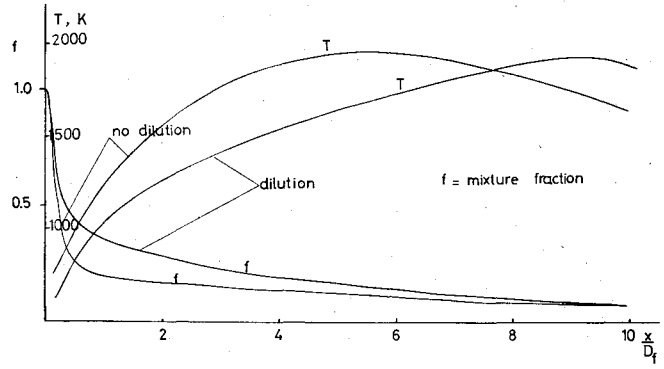

Fig. 8 Effect of dilution air on the centerline distribution of fuel concentration and gas temperature at zero swirl and atmospheric pressure. No dilution case represents the flame situation of Ref. 17.

Profiles of mean gas temperature are shown in Fig. 6; both measured and calculated profiles are in reasonable agreement. In the vicinity of the burner, an off-center peak temperature was observed which coincided with the location of the reaction zone. The comparison shown in Fig. 6 indicated an overall agreement with maximum discrepancies of less than 150 K. The simple calculations, which did not include the density and pressure corrections, resulted in very poor agreement, particularly at $x/D_f = 0.34$, where the predicted temperatures were different from the measurements by up to 300 K in the centerline vicinity.

As can be seen from the temperature distribution at the combustor exit, the flame length is longer than 10 D_f; the measured overall heat flux to the furnace wall contributed to nearly 15% of the total heat input. This is in contrast to the observation in other gas-fired furnaces.[2]

The comparisons shown in Figs. 1-6 illustrate the extent to which calculated values of flow pattern and reaction characteristics can be expected to agree with the measurements. It is clear that discrepancies exist, for example, up to 150 K in temperature and 30% in the size of reversed flow regions, but trends were correctly represented in all cases and the differences are usually considerably smaller. The cost of these calculations is not negligible, but is significantly less than the corresponding experiment. Consequently, the present investigation has been extended to flow situations where no measurements are available.

The present method was further tested in flow situations with dilution air issuing from ports along the combustor of the present study, as shown in Fig. 7. Additional dilution air of an amount equal to that required for combustion is added through two simulated air dilution annular rings. The influence of dilution on the combustor centerline mixture fraction and gas temperature distributions is shown in Fig. 8. Dilution air resulted in a longer and narrower flame. This is just an example of possible parametric studies that can be performed on the combustor for improved alternative design aiming at higher combustion efficiency and lower pollutant emission.

Concluding Remarks

The following conclusions may be drawn from the present investigation.

1) Turbulent diffusion furnace flames can be represented by a four-equation turbulence model, which is based on the k-e model and accounted for the density fluctuation correlations.

2) The combustion model made use of a transport equation for the probability density function of fuel and the calculated probability function is reaction-rate-dependent. The time-averaged reaction rate is equal to the instantaneous rate weighted by the probability density function.

3) The radiative heat-transfer contribution to the total energy balance was represented by the discrete ordinate model.

4) A modification of the pressure correction procedure to account for the effects of high combustor pressure is introduced. The preliminary results obtained here encouraged the adoption of this modification. It should be noted that it cannot be claimed that this modification is in its final form.

5) The incorporation of the density fluctuation terms and correlations in the calculation procedure is essential to adequately calculate, with a reasonable degree of accuracy, the detailed flame structure and pollutant formation rates in high-intensity combustors and furnaces.

6) The present model can be applied to furnace and combustion chamber design. An example of the present capabilities, with simulated wall dilutions, was performed and indicated a longer and narrower flame.

References

[1] Pun, W. M. and Spalding, D. B., "A Procedure for Predicting the Velocity and Temperature Distribution in Confined, Steady, Turbulent, Gaseous, Diffusion Flame," *Proceedings of the 18th International Astronautical Congress,* Belgrade, Yugoslavia, 1967.

[2] Hutchinson, P., Khalil, E. E., and Whitelaw, J. H., "The Measurements and Calculations of Furnace Flow Properties," *Journal of Energy,* Vol. 1, 1977, pp. 212-219.

[3] Khalil, E. E., Spalding, D. B., and Whitelaw, J. H., "The Calculation of Local Flow Properties in Two-Dimensional Furnaces," *International Journal of Heat and Mass Transfer,* Vol. 18, 1975, pp. 775-791.

[4] Khalil, E. E., Hutchinson, P., and Whitelaw, J. H., "The Calculation of Flow and Heat Transfer Characteristics of Gas Fired Furnaces," *Proceedings of the 18th (International) Symposium on Combustion,* 1981, pp. 1927-1938.

[5] Launder, B. E. and Spalding, D. B., "Numerical Computations of Turbulent Flows," *Computer Methods in Applied Mechanics and Engineering,* Vol. 3, 1974, pp. 269-289.

[6] Pope, S. B., "The Calculation of Flows Behind Bluff Bodies With and Without Combustion," Ph.D. Thesis, London University, 1976.

[7] Spalding, D. B., "Concentration Fluctuation in a Round Free Jet," *Chemical Engineering Sciences,* Vol. 26, 1971, pp. 95-110.

[8] Naguib, A. S., "The Prediction of Axisymmetric Free Jet Turbulent Reacting Flows," Ph.D. Thesis, London University, 1975.

[9] Khalil, E. E., "Flow and Combustion in Axisymmetric Furnaces," Ph.D. Thesis, London University, 1977.

[10] Kolbe, W. and Kollmann, W., "Prediction of Turbulent Diffusion Flames with a Four-Equation Turbulence Model," *Acta Astronautica,* Vol. 7, 1980, pp. 91-104.

[11] Khalil, E. E., *Modelling of Furnaces and Combustors,* Abacus Press, 1982.

[12] Khalil, E. E. and Truelove, J. S., "Calculation of Radiative Heat Transfer in a Large Gas-Fired Furnace," *Letters in Heat and Mass Transfer,* Vol. 4, 1977, pp. 353-365.

[13] Spadaccini, L. J., Owen, F. K., and Bowman, C. T., "Influence of Aerodynamic Phenomena on Pollution Formation in Combustion," EPA-600/2-76-247a, 1976.

[14] Khalil, E. E., "Initial and Boundary Conditions and Their Influence on Numerical Computations of Confined Elliptic Flows," *Numerical Methods in Thermal Problems,* edited by Lewis et al., 1979, pp. 458-467.

[15] Launder, B. E., Reece, G. J., and Rodi, W., "Progress in the Development of Reynolds Stress Turbulence Closure," *Journal of Fluid Mechanics,* Vol. 68, 1975, pp. 537-555.

[16] Gosman, A. D. and Pun, W. M., "Calculation of Turbulent Recirculating Flows," Imperial College, London, England, Rept. HTS/74/2, 1974.

[17] Bowman, C. T. and Cohen, L. S., "Influence of Aerodynamic Phenomena on Pollutant Formation in Combustion, Experimental Results," EPA-650/2-75-061-2, 1975.